Journal for ImmunoTherapy of Cancer

B4GALT5 inhibits CD8+ T-cell response by downregulating MHC-I level through ERAD pathway in PDAC

Xin Xing ,[1,2] Shi-Qi Yin,[1] Xia-Qing Li,[1] Hui Li,[3] Hong-Tai Ma,[1] Aziguli Tulamaiti,[3] Shu-Yu Xiao,[3] Yu-Tong Liu,[4] Hao Zhang,[5] Zhigang Zhang,[3] Yan-Miao Huo,[6] Xiao-Mei Yang,[3] Yan Yang,[3] Xue-Li Zhang [2,3]

To cite: Xing X, Yin S-Q, Li X-Q, *et al*. B4GALT5 inhibits CD8+ T-cell response by downregulating MHC-I level through ERAD pathway in PDAC. *Journal for ImmunoTherapy of Cancer* 2025;**13**:e010908. doi:10.1136/jitc-2024-010908

► Additional supplemental material is published online only. To view, please visit the journal online (https://doi.org/10.1136/jitc-2024-010908).

XX, S-QY, X-QL and HL contributed equally.

Accepted 17 April 2025

For numbered affiliations see end of article.

Correspondence to
Dr Xue-Li Zhang;
xlzhang@shsci.org

Dr Yan Yang;
yangyang201298@163.com

Dr Xiao-Mei Yang;
xmyang@shsci.org

Dr Yan-Miao Huo;
huoyanmiao@126.com

ABSTRACT

Background Immune evasion is a crucial event in the progression of pancreatic ductal adenocarcinoma (PDAC). The identification of new immunotherapeutic targets may provide a promising platform for advancing PDAC treatment. This study aims to investigate the role of beta-1,4-galactosyltransferase-5 (B4GALT5) in immune evasion by pancreatic cancer cells and evaluate its potential as an immunotherapeutic target.

Methods We conducted a comprehensive analysis using RNA sequencing data and tissue microarrays from patients with PDAC to investigate the association between B4GALT5 expression and patient prognosis. Using animal models, we further explored the impact of B4GALT5 on the quantity and activity of tumor-infiltrating CD8+ T cells. RNA sequencing and co-immunoprecipitation were used to explore the mechanism by which B4GALT5 regulates major histocompatibility complex (MHC-I) levels.

Results Our study demonstrates that high expression of B4GALT5 in tumor cells is significantly associated with poor prognosis in patients with PDAC and reduced cytotoxic activity of tumor-infiltrating CD8+ T cells. Specifically, B4GALT5 suppresses MHC-I expression in tumor cells through the endoplasmic reticulum-associated degradation pathway, enabling them to evade immune surveillance by CD8+ T cells.

Conclusions B4GALT5 impairs CD8+ T-cell recognition of tumor cells by regulating MHC-I levels, thereby promoting immune evasion. This makes B4GALT5 a highly promising immunotherapeutic target for improving the poor prognosis of patients with PDAC.

WHAT IS ALREADY KNOWN ON THIS TOPIC

⇒ Pancreatic ductal adenocarcinoma (PDAC) cells often downregulate major histocompatibility complex (MHC)-I on their surface, enabling them to evade immune surveillance, leading to immune evasion and even resistance to immune checkpoint inhibitor therapy.

WHAT THIS STUDY ADDS

⇒ This study first identifies beta-1,4-galactosyltransferase-5 (B4GALT5) as a novel negative regulator of MHC-I in PDAC, which promotes the ubiquitination and degradation of MHC-I via the endoplasmic reticulum-associated degradation (ERAD) pathway, ultimately impairing antigen presentation and suppressing CD8+ T cell responses.

HOW THIS STUDY MIGHT AFFECT RESEARCH, PRACTICE OR POLICY

⇒ By highlighting B4GALT5 as a key driver of immune evasion in PDAC, this study demonstrates that targeting B4GALT5 can restore MHC-I expression, enhance CD8+ T cell responses, and improve the efficacy of immunotherapy, providing a promising therapeutic target for PDAC treatment, potentially revolutionizing current treatment strategies.

INTRODUCTION

Pancreatic ductal adenocarcinoma (PDAC) accounts for over 90% of pancreatic cancer and is one of the most challenging malignancies of the digestive system. Despite significant advances in surgery, radiotherapy, chemotherapy, and comprehensive treatment methods, the prognosis and overall mortality rate for patients with PDAC have only improved marginally.[1 2] Pancreatic cancer cells often downregulate major histocompatibility complex (MHC)-I on their surface, thereby evading host immune surveillance and facilitating immune escape, which promotes resistance to immune checkpoint inhibitor therapies and is a significant factor in poor clinical outcomes.[3 4] Therefore, a deep understanding of the molecular mechanisms behind tumor cell immune evasion is crucial for revealing new tumor immune targets and developing effective tumor treatment strategies.

Under normal circumstances, MHC-I molecules help the immune system monitor and maintain healthy body states by presenting normal peptides from intracellular proteins, preventing viral infections or the spread of tumor cells.[5] However, in most PDAC cells, the expression of MHC-I molecules is often suppressed, allowing tumor cells to more

easily evade recognition and killing by $CD8^+$ T cells, thus facilitating their growth and spread in the body. This immune evasion caused by tumor cells is one of the challenges that need to be overcome in cancer therapy.[4 6 7]

Recent studies have demonstrated that glycosyltransferases play a significant role in regulating protein glycosylation, thus having a profound impact on cancer development.[8 9] The abnormal expression of these enzymes directly affects various biological characteristics of tumors, including cell signaling, tumor cell invasion and metastasis, as well as immune modulation functions.[10 11] Their abnormal expression or activity is often associated with tumor malignancy. Therefore, glycosyltransferases themselves or their glycosylation products can serve as biomarkers for diagnosing tumors, monitoring disease progression, or treatment response.[12 13]

Beta-1,4-galactosyltransferase-5 (B4GALT5), an important member of the beta-1,4-galactosyltransferase gene family, encodes a type II membrane-bound glycoprotein with specificity for the donor substrate uridine diphosphate (UDP) galactose. Each beta-1,4-galactosyltransferase gene plays a unique role in the biosynthesis of various glycoconjugates and sugar structures. As type II membrane proteins, they have an N-terminal hydrophobic signal sequence responsible for protein transfer to the Golgi and serve as a transmembrane anchor.[14] Previous studies have shown that B4GALT5 plays an irreplaceable role in diabetes and heart disease. For example, B4GALT5 can regulate adipogenesis and inhibit M1 macrophage infiltration, thereby modulating insulin resistance.[15] B4GALT5 and UDP-glucose ceramide glycosyltransferase (UGCG) synergistically play important roles in the occurrence and development of myocardial hypertrophy.[16] Although *B4GALT5* expression is significantly increased in PDAC,[17] its potential role has not yet been explored. In this study, we revealed that B4GALT5 interacted with the MHC-I heavy chain, hindering its assembly with beta-2 microglobulin (B2M), thus leading to its degradation via the endoplasmic reticulum-associated degradation (ERAD) pathway. This allows tumor cells to more easily evade surveillance by the host immune system, ultimately leading to immune escape by the tumor cells. Furthermore, we have validated *in vitro* and *in vivo* that knocking out *B4GALT5* significantly improves the activity of $CD8^+$ T cells, indicating the important clinical significance of B4GALT5 in pancreatic cancer immunotherapy.

METHODS

Data mining and bioinformatics analysis

Based on a gene signature consisting of eight genes (HLA-A, HLA-E, HLA-F, HLA-G, HLA-H, AZGP1, B2M and TAP2). Derived from the MSigDB database associated with "antigen processing and presentation of peptide antigen via MHC-I", the enrichment scores for each sample were calculated using Gene Set Variation Analysis (GSVA) on the expression matrix for 143 PDAC samples from The Cancer Genome Atlas (TCGA) database. Samples were divided into high-risk and low-risk groups based on the median value. The differentially expressed genes (DEGs) between high-risk and low-risk groups were identified using the two-tailed Wilcoxon signed-rank test and false discovery rate correction procedure (Benjamini-Hochberg method), and the fold change (log_2FC) between the two groups was calculated. TCGA-PDAC plus GTEx database (the latter includes normal pancreatic samples), and two Gene Expression Omnibus data sets (GSE16515 and GSE28735) were used in this study to determine the expression of different genes.

CIBERSORT V.1.03 was employed to assess immune cell infiltration in each sample based on RNA sequencing (RNA-seq) data from 143 PDAC samples obtained from the TCGA database. After obtaining immune infiltration scores for each sample, Spearman correlation coefficient analysis was used to evaluate the relationship between B4GALT5 expression and immune cell infiltration. Three publicly available single-cell RNA-seq (scRNA-seq) data sets from GSE212461, GSE202051 and GSE156405 were used to analyze the messenger RNA (mRNA) expression of B4GALT5 across different cell types under different conditions. Cell clustering analysis was conducted by Seurat V.4.4.0 with default parameters.

Clinical samples

The 100 tissue samples used to construct the tissue microarray were collected from patients treated surgically for PDAC at the Department of Hepatobiliary Surgery, Ren Ji Hospital, affiliated with Shanghai Jiao Tong University, and were confirmed by postoperative pathology. All tissue samples were obtained with informed consent, and all procedures were conducted in accordance with the regulations of the China Ethical Review Committee. Follow-up time was calculated from the date of surgery to the date of death related to pancreatic cancer or the last known follow-up date. Relevant information is provided in online supplemental table 1.

Cell culture

Human PDAC cell lines (PATU8988, PANC-1, MIA-PaCa-2, SW1990, Capan-1, AsPC-1, and CFPAC-1), along with the human pancreatic ductal cell line HPNE, and mouse PDAC cell lines KPC1199 and PANC02, were preserved in Shanghai Cancer Institute, Shanghai Jiao Tong University, and maintained at 37°C. All cell lines were cultured in Roswell Park Memorial Institute medium 1640 (RPMI-1640) or Dulbecco's Modified Eagle Medium (DMEM) supplemented with 10% fetal bovine serum (FBS) and 1% antibiotic additives. The cells were incubated at 37°C in a humidified atmosphere with 5% CO_2.

Transient transfection

Small interfering RNA (siRNA) duplex oligonucleotides targeting human B4GALT5 were purchased from Biotend Biotechnology (Shanghai, China). The siRNA duplex oligonucleotide sequences are si-*B4GALT5*-1: 5'-GACATGAAACAUGAGUGAAATT-3'; si-*B4GALT5*-2:

5'-GCTTATGCCAAGAGGAACATT-3'. Multiple plasmids were purchased from several companies, among them, pcDNA3.1(+)-B4GALT5-3xFlag and the negative control plasmid pcDNA3.1(+)-MCS-3xFlag were purchased from Obio Technology (Shanghai, China); pcDNA3.1(+) HLA-A0201-N110Q-3xFlag was purchased from Bio-lifespan (Shanghai, China). Transfection was carried out using JetPRIME (Polyplus transfection, 101000046) according to the manufacturer's instructions.

Stable cell line construction

Lentiviral particles targeting the mouse sh-*B4galt5* gene were purchased from Obio Technology (Shanghai, China). The sequences used for knocking down B4galt5 are: sh-*B4galt5*-1, 5'-CATACCTGAGAGTGACCGAAA-3'; sh-*B4galt5*-2, 5'GCAGCCTGAATGACTCAGATT-3'. Lentiviral particles for overexpression targeting human *HLA-A2* (XM_041680767.1) were purchased from Bio-lifespan (Shanghai, China). Lentiviral particles for overexpression of mouse OVA were purchased from GeneChem (Shanghai, China). Cells were cultured in 6-well plates and transfected with lentiviral particles in the presence of polybrene when they reached 50% confluence, following the manufacturer's instructions. After 48 hours of transfection, the cells were treated with 2 µg/mL puromycin (Yeasen, 60210ES60) for 7 days to select stable knockdown or overexpressing cells.

Quantitative real-time PCR

Total RNA extraction was conducted using TRIzol reagent (Takara), followed by reverse transcription to obtain complementary DNA (cDNA). Quantitative real-time PCR was performed using a 7500 Real-Time PCR system (Applied Biosystems, USA) with recommended cycling settings. The cycling conditions included an initial cycle at 95°C for 2 min, followed by 35 cycles of 5 s at 95°C and 31 s at 60°C. The 2-ΔCT method was employed for evaluation and normalization, with 18S mRNA levels used for relative mRNA expression calculations. The primers mentioned are listed in online supplemental table 2.

Western blotting

For cell protein extraction, cells were lysed in Cell Lysis Buffer for western and IP (Yoche; YSD0101) supplemented with Protease and Phosphatase Inhibitor Cocktail (New Cell and Molecular Biotech; P002) on ice for 10 min, followed by centrifugation at 12,000 rpm for 15 min at 4°C. The supernatants were collected, and the protein concentration was determined using a BCA Protein Assay Kit (share-bio, SB-WB013) followed by standardization. Subsequently, 5×SDS PAGE Sample Loading Buffer (Beyotime; P0015) was added, and the samples were boiled in a water bath for 10 min. Protein lysates were separated via 8–12% sodium dodecyl sulfate-polyacrylamide gel electrophoresis (SDS-PAGE) and transferred onto nitrocellulose (NC) membranes. After blocking for non-specific binding with 5% non-fat dried milk, the membranes were incubated with primary antibodies overnight at 4°C, followed by incubation with a horseradish peroxidase (HRP) conjugated secondary antibody. Detailed information on antibodies is listed in online supplemental table 3.

Co-immunoprecipitation

Cells expressing or not expressing B4GALT5-Flag and HLA-A-HA were lysed according to the western blot (WB) method previously described, and protein quantification was performed using the bicinchoninic acid (BCA) method. Immunoprecipitation was carried out with Anti-Flag (Selleck, B26102) or Anti-Ha magnetic beads (Thermo Fisher Scientific, 88836) by rotating continuously at 4°C for 12 hours. The beads were then thoroughly washed with phosphate-buffered saline (PBS) containing 0.1% Tween, followed by the addition of SDS sample buffer. The proteins were dissociated from the beads by heating at 100°C for 10 min, and the supernatant was collected for mass spectrometry analysis (Bioprofile, Shanghai, China) or WB analysis.

RNA sequencing

Total RNA was extracted from AsPC-1 cells in the NC and si-*B4GALT5* groups using TRIzol (Takara). Poly(A) RNA was isolated from 1 µg total RNA, and a cDNA library was generated according to the protocol of the TruSeq RNA Sample Prep Kit. Subsequently, sequencing was performed using the Illumina NovaSeq 6000 platform. For RNA-seq analysis, paired-end clean reads were aligned to the human reference genome (GRCh38) using HISAT2. The aligned reads were then used to quantify mRNA expression, and DESeq2 was used for data normalization and differential expression analysis of RNA-seq counts. The raw RNA-seq data has been uploaded to the public database (GSE285130).

Animal studies

Mice were housed and used according to protocols approved by the Shanghai Jiao Tong University Animal Care Commission. All animals received humane care according to the criteria outlined in the "Guide for the Care and Use of Laboratory Animals" prepared by the National Academy of Sciences and published by the National Institutes of Health (NIH).

The counted tumor cells (KPC1199=6×10^5, PANC02=1×10^6) were suspended in 25 µL PBS and implanted into the pancreas of C57BL/6J mice following surgical exposure. Tumor progression in the mice was monitored on days 7, 14, 21, and 28 using the living image system.

In the H-2Kb blocking experiment in mice, the orthotopic PDAC model was divided into four groups: IgG sh-NC group, IgG sh-*B4galt5* group, αH-2Kb sh-NC group, and αH-2Kb sh-*B4galt5* group. Starting from day 3 after model establishment, mice were administered anti-H-2Kb antibody or IgG isotype control antibody (200 µg) via intraperitoneal injection every 3 days. At the end of the experiment, mice were euthanized, and tumor tissues

were collected for analysis to evaluate the therapeutic effect of H-2Kb blockade.

Co-culture experiments

36 hours prior to co-culture, tumor cells were seeded into a 24-well plate (2×10^4/well) and a 96-well plate (3×10^3/well). $CD8^+$ T cells from the spleen of OT-1 mice (the OT-1 mice were generously provided by Professor Minjuan Xu of Shanghai Jiao Tong University) were isolated using $CD8^+$ T Cell Isolation Beads (Miltenyi, 130-104-453). Primary $CD8^+$ T cells were activated with αCD3 (5 µg/mL) and αCD28 (2 µg/mL) antibodies in RPMI 1640 medium supplemented with 10% FBS, and cultured at 37°C with 5% CO_2 for 36 hours. Different ratios of immune cells were then added to the tumor cells in the 24-well and 96-well plates for co-culture. After 24 hours of co-culture, the suspended $CD8^+$ T cells were removed, and the plates were washed three times with PBS. According to the manufacturer's instructions, tumor cell apoptosis was assessed using an Apoptosis Assay Kit (Share-Bio, SB-Y6026) by flow cytometry. Tumor cell viability was assessed using a Cell Counting Kit-8 (CCK8) assay kit (Share-Bio, SB-CCK8S).

KPC1199-OVA cells with different B4GALT5 expression levels were incubated at 4°C with either H-2Kb-SIINFEKL antibody or IgG control antibody (100 µg/mL) for 30 min. Subsequently, activated OT-1 $CD8^+$ T cells were co-cultured with the tumor cells at a 5:1 ratio for 12 hours. The cytotoxic activity of $CD8^+$ T cells was then assessed using flow cytometry.

ELISA

Activated OT-1 $CD8^+$ T cells were co-cultured with KPC1199-OVA and PANC02-OVA cells for 12 hours. Subsequently, the cell culture supernatants were collected and analyzed using GZMB (Animalunion Biotechnology, LV30229), TNF-α (Animalunion Biotechnology, LV30536), and IFN-γ (Animalunion Biotechnology, LV30253) ELISA kits, following the manufacturer's instructions. Finally, the absorbance was measured at 450 nm using a microplate reader to quantify the expression levels of the target molecules.

Flow cytometry

Adherent tumor cells were digested with trypsin, and the digestion was stopped with DMEM complete medium containing 10% FBS. The cells were then transferred to a 1.5 mL Eppendorf tube. Using FACS Buffer (2% FBS in PBS), fluorescently labeled antibodies against human HLA-ABC, mouse H-2Kb, and OVA257-264 were diluted at a 1:200 ratio. The diluted antibodies were incubated with the cells at 4°C for 30 min. After incubation, 500 µL of FACS Buffer was added, followed by centrifugation at 4°C at 3,000 rpm for 5 min. The supernatant was discarded, and the cells were resuspended in 300 µL of FACS Buffer before being transferred to a flow cytometry tube.

For the analysis of tumor-infiltrating $CD8^+$ T cells, on day 28 of the mouse PDAC model, the mice were euthanized, and fresh tumor tissues were collected. The tissues were cut into small pieces with surgical scissors and then digested with collagenase D (Sigma) for 20 min, neutralized with FBS (Gibco), and filtered through a 70 µm nylon filter to obtain a single-cell suspension. Tumor-infiltrating T cells were isolated by centrifugation over a Ficoll gradient. To assess the function of $CD8^+$ T cells, cells were first stimulated for 4 hours in the presence of a leukocyte activation cocktail (BD, 550583). For cell surface fluorescence staining, antibodies against CD45, S780, and CD8 were used. For intracellular fluorescence staining, the cells were first fixed and permeabilized with 4% Paraformaldehyde (PFA) Fix Solution, then stained with fluorescein-labeled granzyme B (GZMB), Tumour necrosis factor (TNF)-α, and interferon (IFN)-γ. Flow cytometry analysis was conducted using a BD Fortessa FACS with FlowJo software V.10.8.

Immunohistochemistry

Tumor tissues were fixed in 4% PFA, followed by tissue dehydration, embedding in paraffin, and subsequent sectioning into 5 µm thick slices. These sections were then incubated in 10% bovine serum albumin (BSA) after antigen retrieval, and primary antibodies were applied at optimal dilutions overnight at 4°C. Afterward, the sections were treated with an HRP-labeled secondary antibody for 1 hour at room temperature. Color development was achieved using 3,3'-Diaminobenzidine (DAB, servicebio, G1212-200T). Finally, the sections were counterstained with hematoxylin for visualization. All sections were examined and photographed using a microscope (Carl Zeiss, Germany). The calculation formula for the histochemistry score is as previously described.[18 19]

Multiplexed immunohistochemistry

Multiplexed immunohistochemistry (mIHC) was performed using the TSA 7-Color Kit (abs50015-100T, Absinbio, Shanghai). Following the standard immunohistochemistry protocol described above, sequential staining was performed with the following primary antibodies and fluorescent dyes: anti-B4GALT5/TSA 570, anti-CD8/TSA 520, anti-GZMB/TSA 480, and anti-HLA-A B C/TSA 620, with DAPI used for nuclear staining. Finally, two drops of DAPI (abs47047616, Absinbio, Shanghai) were added to each slide, followed by washing with distilled water and manual coverslipping.

Immunofluorescence

Tissue sections underwent heat-mediated antigen retrieval in sodium citrate buffer solution at pH 6.0 for 10 min. Subsequently, they were blocked with 10% BSA and co-incubated overnight at 4°C with primary antibodies at optimal dilutions. For cell staining, sections were fixed in 4% formaldehyde for 10 min at room temperature, permeabilized with 0.1% Triton X-100 for 10 min, and blocked with 3% BSA. Primary antibody incubation occurred overnight at 4°C. Following primary antibody incubation, sections were treated with a species-specific

secondary antibody for 1 hour at room temperature. 4',6-diamidino-2'-phenylindole (DAPI) staining was applied for 5 min to label nuclei. After three washes with 1×PBS, immunofluorescence signals were visualized using confocal microscopy (Carl Zeiss).

Statistical analysis

Data are presented as mean±SD. All statistics were carried out using GraphPad Prism V.8. Student's t-test was used to compare the differences between two groups. One-way analysis of variance and Tukey's multiple comparisons test were used for the three or more groups comparisons. At least three independent biological replicates have been performed for each experiment. Survival analysis was done using the Kaplan-Meier method, as assessed using a log-rank Mantel-Cox test. The number of independent experiments is indicated. P value<0.05 was considered to be statistically significant.

RESULTS

B4GALT5, as a potential negative regulator of MHC-I, is highly expressed in PDAC and negatively correlates with prognosis

To analyze the potential negative regulators of MHC-I in PDAC, we scored 143 PDAC samples from the TCGA database using the GSVA algorithm based on an eight-gene "antigen processing and presentation of peptide antigen via MHC-I" signature.[20] Based on these scores, we categorized PDAC samples into two groups (high risk vs low risk) and identified 117 DEGs that negatively correlated with MHC-I (online supplemental figure S1A, online supplemental table 4). Among these DEGs, several top genes, such as *MUC2*, *MAGEC2*, *MMP1* and *IDO1*, have also been identified by other research groups as negative regulators of MHC-I, demonstrating the reliability of our analysis.[21–24] Additionally, we conducted differential analysis on 50 paired cancer and adjacent normal RNA-seq data from Renji Hospital,[25] along with paired data from GSE16515[26] and GSE28735,[27] to identify genes significantly upregulated in tumor tissues. By integrating the above data and considering the clinical information provided by the TCGA database, we ultimately identified four candidate genes (*ADAM9*, *B4GALT5*, *ECT2*, and *TUBA1C*) (figure 1A–E, online supplemental figure S1B-D). Notably, *ADAM9* has been reported to promote PDAC progression by modulating *KRAS*.[28] *ECT2* plays a significant role in PDAC progression by increasing EGFR stability through the inhibition of Grb2 ubiquitination.[29] *TUBA1C* may promote PDAC invasion and migration via the cell cycle.[30] Given the known roles of these three candidates, we focused on investigating the function of *B4GALT5* in PDAC in our study.

To explore the expression pattern of B4GALT5 in PDAC, we analyzed the scRNA-seq data from GSE212461[31] of PDAC tumor tissues, which revealed that B4GALT5 is primarily expressed in tumor cells (figure 1F). To further ascertain the expression of the B4GALT5 protein, we performed immunohistochemical (IHC) staining on pancreatic cancer tissue microarrays from the Department of Hepatobiliary and Pancreatic Surgery at Renji Hospital. We found that B4GALT5 expression increased from normal pancreas to PanINs and PDAC, and B4GALT5 expression is significantly positively correlated with tumor size in patients (figure 1G and online supplemental figure S2A). Additionally, combining the clinical information, survival analysis showed that B4GALT5 expression was significantly negatively correlated with patient prognosis, which was consistent with previous analyses (figure 1H). Furthermore, KPC mice exhibited a higher expression of B4GALT5 in tumor tissues compared with normal pancreatic tissue (figure 1I).

B4GALT5 promotes PDAC progression *in vivo*

To further validate the impact of B4GALT5 expression on the progression of pancreatic cancer, we knocked down the expression of *B4galt5* in murine pancreatic cancer cells KPC1199 and PANC02 cells (figure 2A,B), while simultaneously transfecting them with the luciferase fluorescent protein for observation of tumor progression in mice using the living image system. We established a murine pancreatic cancer orthotopic model in C57BL/6 mice and monitored tumor progression in the mice every 7 days. The results showed that knocking down *B4galt5* significantly inhibited tumor progression (figure 2C,D). Tumors were harvested on day 28, and their size and weight were measured. The results also indicated a significant reduction in tumor size and weight in the sh-*B4galt5* group compared with the sh-NC group (figure 2E,F). Additionally, we performed Cleaved Caspase-3 staining on tumor tissues and found that the number of Cleaved Caspase-3^{+} cells was significantly higher in the sh-*B4galt5* group than in the sh-NC group, indicating that *B4galt5* knockdown significantly promotes tumor cell apoptosis (figure 2G,H, online supplemental figure S2B,C).

B4GALT5 suppresses the presentation of MHC-I molecules on PDAC cell membrane

The above results suggest that B4GALT5 plays an important role in the progression of pancreatic cancer. To verify whether *B4GALT5* promotes the progression of pancreatic cancer by affecting MHC-I-mediated antigen presentation, we analyzed the expression levels of H-2Kb (murine MHC-I) on the surface of murine PDAC cells (KPC1199 and PANC02) in both sh-NC and sh-*B4galt5* groups using flow cytometry. The results revealed that the expression level of H-2Kb was significantly elevated on the surface of murine PDAC cells after knocking down *B4galt5* (figure 3A and online supplemental figure S3A). Furthermore, we checked the expression of B4GALT5 in human pancreatic cancer cell lines and normal duct cells (HPNE) (online supplemental figure S3B,C). We then knocked down the expression of *B4GALT5* in AsPC-1 and Capan-1 cells, which have relatively high *B4GALT5* expression, while exogenously overexpressing *B4GALT5* in PANC1 and MIA-PaCa-2 cells, which have relatively low *B4GALT5* expression (figure 3B,C and

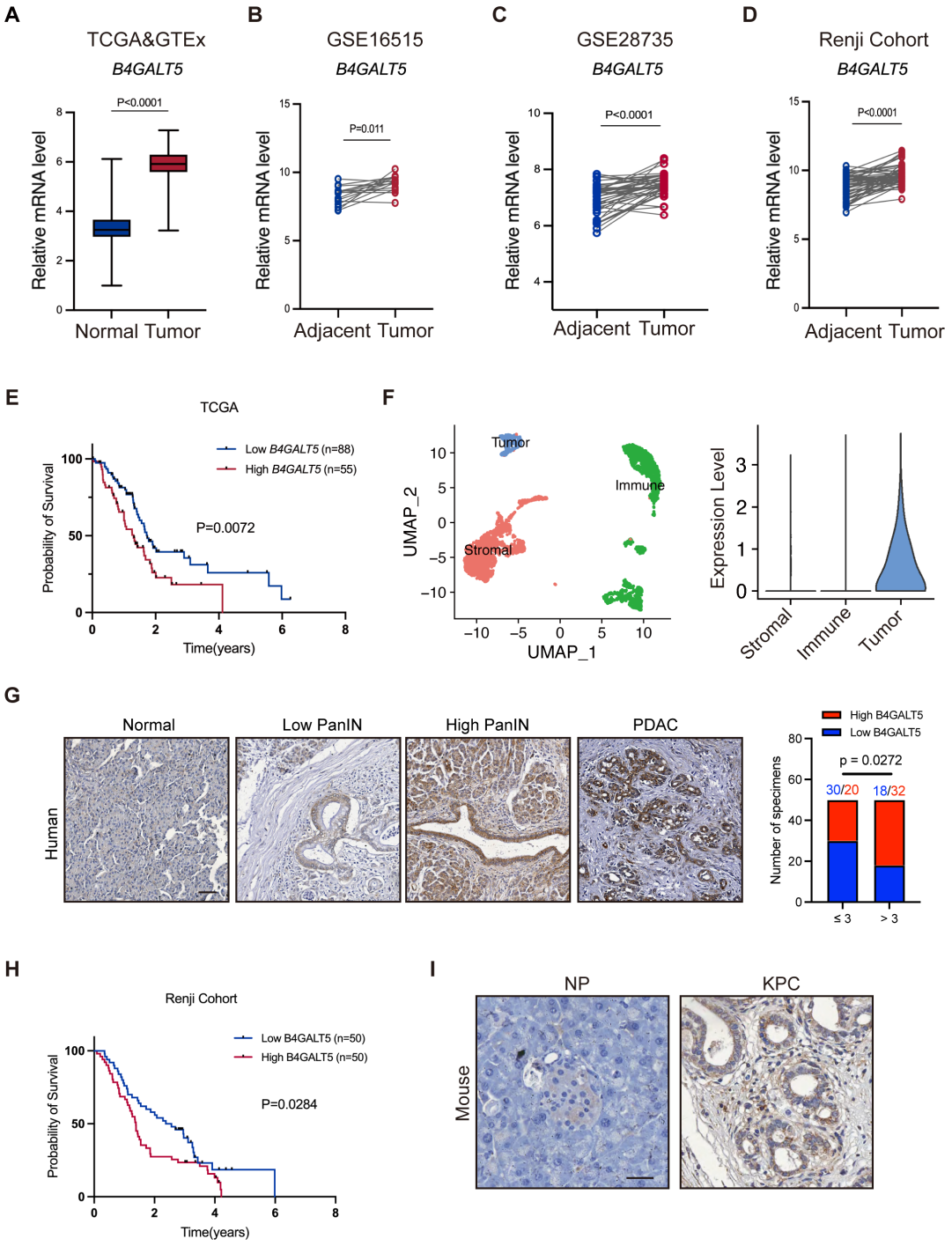

Figure 1 B4GALT5 is highly expressed and predicts a poor prognosis in PDAC. (A) Differences in *B4GALT5* mRNA expression between normal pancreatic tissues and tumor tissues in the TCGA and GTEx databases. (normal=171, tumor=143). (B–D) Differences in *B4GALT5* mRNA expression between adjacent normal tissue and tumor tissue. GSE16515 (B, n=16 per group); GSE28735 (C, n=45 per group); Renji cohort (D, n=50 per group). (E) KM survival curves (log-rank test) comparing overall survival between high *B4GALT5* expression samples (n=55) and low expression samples (n=88) in PDAC by using TCGA database. (F) Quantitative analysis of *B4GALT5* mRNA expression in stromal cells, immune cells, and tumor cells in the GSE212461 single-cell RNA sequencing data set using log2 (TPM+1). (G) Left: representative immunohistochemical staining images showing differences in B4GALT5 expression from normal pancreas, through PanIN stages to PDAC (Scale bar: 50 µm). Right: correlation analysis of B4GALT5 expression with tumor size of patients with PDAC from Renji cohort (Fisher's exact test). (H) Analysis of the relationship between B4GALT5 expression and patient prognosis based on immunohistochemical staining of patient with PDAC tissue microarrays from Renji Hospital, combined with clinical information using KM survival curves (log-rank test) (n=50 per group). (I) Representative immunohistochemical images showing differences in B4GALT5 expression between normal C57BL/6 mouse pancreas (NP) and KPC mouse pancreas (scale bar: 50 µm). B4GALT5, beta-1,4-galactosyltransferase-5; mRNA, messenger RNA; PDAC, pancreatic ductal adenocarcinoma; TCGA, The Cancer Genome Atla; KM, Kaplan-Meie; TPM, Transcript per million.

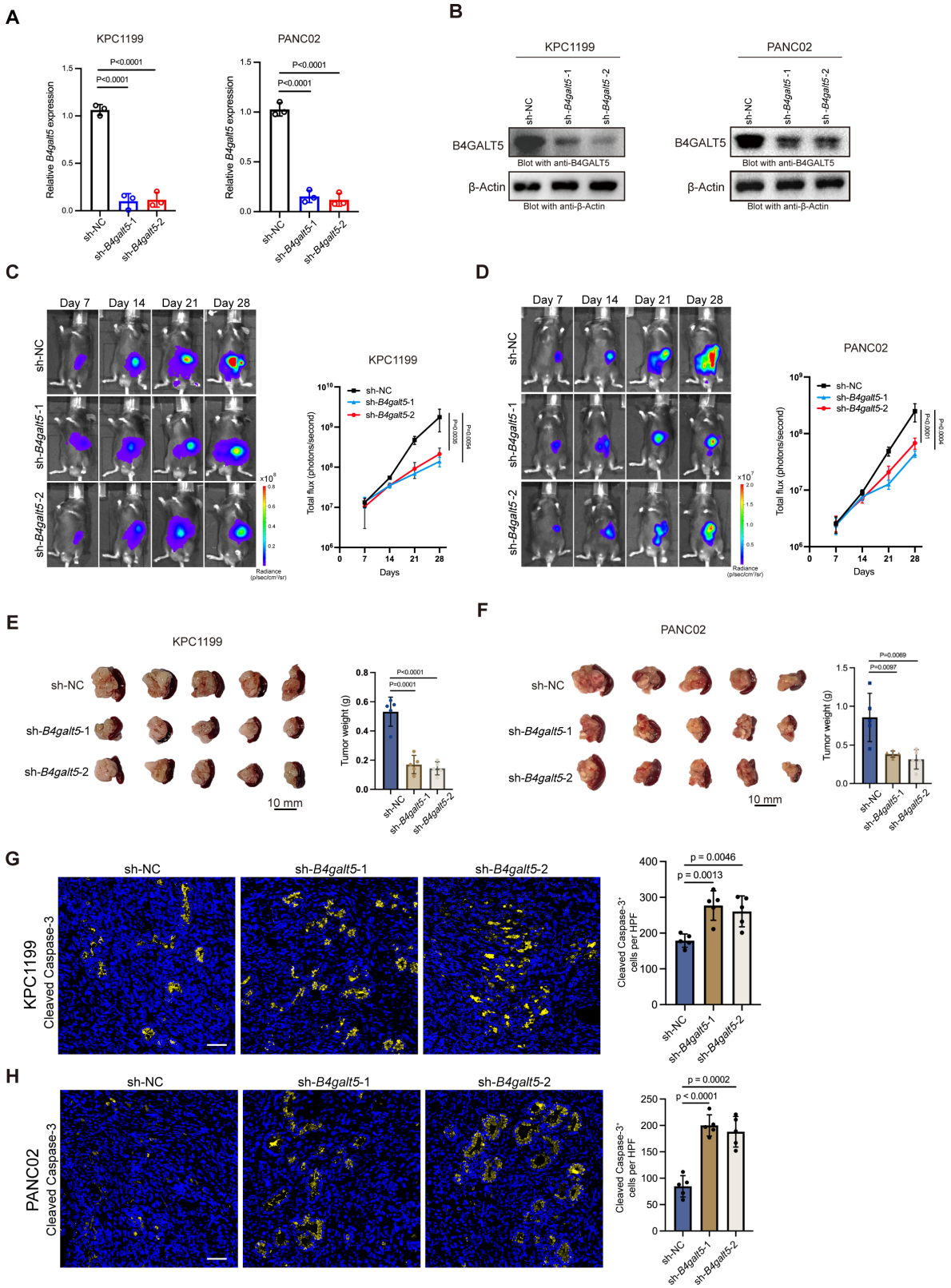

Figure 2 B4GALT5 promotes PDAC progression *in vivo*. (A–B) Verification of *B4galt5* knockdown efficiency by quantitative PCR (A) and western blot (B) in KPC1199 and PANC02 cell lines. (C–D) Living Image system used to observe the progression of tumors in orthotopic PDAC mouse models using KPC1199 (C) and PANC02 (D) cells. n=5, per group. (E–F) Tumor size and weight on day 28 were analyzed. KPC1199 (E), PANC02 (F). (G–H) Immunofluorescence detection of Cleaved Caspase-3^{+} cells in the sh-NC and sh-*B4galt5* groups of mouse PDAC models inoculated with the KPC1199 (G) and PANC02 cells (H), respectively. n=5, per group. Bars represent mean±SD. The p values presented, except for those in C and E, were calculated using an unpaired t-test. The p values for C and E were derived from a two-way analysis of variance. B4GALT5, beta-1,4-galactosyltransferase-5; PDAC, pancreatic ductal adenocarcinoma.

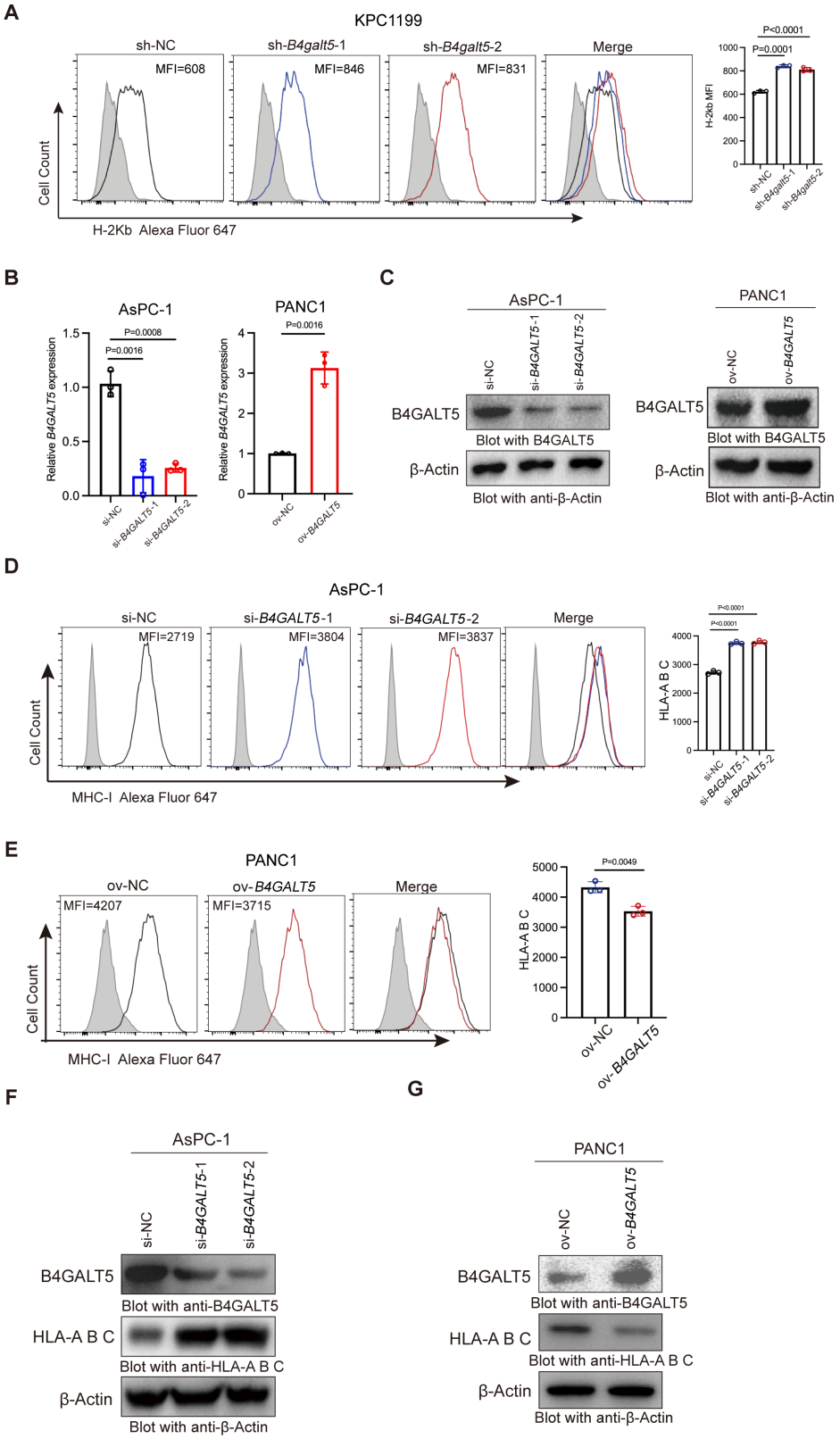

Figure 3 B4GALT5 suppresses the presentation of MHC-I molecules on PDAC cell membrane. (A) Flow cytometry analysis of H-2Kb levels on the surface of KPC1199 mouse PDAC cells in sh-NC and sh-*B4galt5* groups. n=3 per group, three independent experiments. (B–C) Verification of knockdown and overexpression efficiency of *B4GALT5* by quantitative PCR (B) and western blot (C) in AsPC-1 and PANC1. (D–E) Flow cytometry analysis of the alteration of the MHC-I level on the cell surface after *B4GALT5* knockdown in AsPC-1 cells (D) and overexpression in PANC1 cells (E). (F–G) Western blot analysis of the alteration of total HLA-A, B, C protein levels after *B4GALT5* knockdown in AsPC-1 cells (F) and overexpression in PANC1 cells (G). Bars represent mean±SD. The p values shown were calculated using an unpaired t-test. B4GALT5, beta-1,4-galactosyltransferase-5; MHC, major histocompatibility complex; PDAC, pancreatic ductal adenocarcinoma.

online supplemental figure S3D,E). Flow cytometry analysis revealed that knocking down *B4GALT5* significantly increased MHC-I expression on the cell membrane, while overexpressing *B4GALT5* led to a marked decrease in its expression. These results are consistent with observations in murine cells (figure 3D,E and online supplemental figure S3F,G). We also extracted total cellular protein and performed WB analysis. We found that total MHC-I protein levels significantly increased following B4GALT5 knockdown but decreased with B4GALT5 overexpression (figure 3F,G and online supplemental figure S3H,I). Therefore, the results above suggest that B4GALT5 can inhibit the protein level of MHC-I in tumor cells, thereby promoting the progression of PDAC.

B4GALT5 regulates MHC-I via endoplasmic reticulum-associated degradation pathway

To further investigate the underlying molecular mechanism by which B4GALT5 influences MHC-I expression, we performed RNA-seq analysis in AsPC-1 cells with *B4GALT5* knockdown. We found that in 1,660 DEGs, 1,030 genes had significantly increased expression, while 630 genes had significantly decreased expression (online supplemental figure S4A,B). Gene Ontology enrichment analysis of these DEGs revealed that knocking down *B4GALT5* activated several ubiquitin and endoplasmic reticulum (ER)-related pathways (figure 4A). By confocal microscopy, we observed that B4GALT5 is predominantly expressed in proximity to the nuclear, with remarkable colocalization with the ER marker calnexin (CANX) (figure 4B). It is well known that after translation, MHC-I is transported to the ER via the SEC61 complex.[32] After glycosylation and folding with molecular chaperones like CANX, MHC-I forms a mature complex with B2M. The mature MHC-I then binds antigen peptides delivered by tapasin and is finally transported to the cell surface through the Golgi apparatus for $CD8^+$ T cells to recognize via their T-cell receptor.[5] If the proteins synthesized in the ER cannot fold or undergo glycosylation correctly, they enter the ERAD pathway for ubiquitination and degradation by the proteasome.[6 33 34]

We further established stable cell lines of AsPC-1 and Mia-PaCa-2 pancreatic cancer cells overexpressing HLA-A-HA. Subsequently, we manipulated the expression of B4GALT5 and examined the ubiquitination level of HLA-A-HA. The results showed that knocking down *B4GALT5* significantly reduced the ubiquitination levels of HLA-A, whereas overexpression of *B4GALT5* significantly increased them (figure 4C). This indicates that B4GALT5 expression affects the ubiquitination of HLA-A. To confirm whether the expression of *B4GALT5* promotes the degradation of HLA-A, we treated the AsPC-1 cells (both si-NC and si-*B4GALT5* groups) with cycloheximide (10 µM) for 0, 2, 4, and 6 hours, collected the whole cell lysates, and detected HLA-A protein levels via WB. We found that knocking down *B4GALT5* significantly prolonged the half-life of HLA-A (figure 4D). The results indicate that knocking down *B4GALT5* significantly reduced the ubiquitination level of HLA-A, whereas overexpressing *B4GALT5* significantly increased the ubiquitination level of HLA-A.

Next, using PANC1 cells overexpressing B4GALT5-Flag, we extracted total cell lysates, and performed immunoprecipitation-mass spectrometry (IP-MS) analysis. We identified several proteins that interact with B4GALT5, including HLA-A (online supplemental figure S4C). Interestingly, further validation through co-immunoprecipitation (Co-IP) revealed that B4GALT5 not only interacts with HLA-A (figure 4E) but also with SEC61A, an important transporter of MHC-I (figure 4F). Thus, we hypothesized that the degradation of HLA-A could be due to the interaction between B4GALT5 and HLA-A. To verify this hypothesis, we manipulated B4GALT5 expression in pancreatic cancer cells AsPC-1 and MIA-PaCa-1, which overexpressed HLA-A-HA, and assessed the binding of HLA-A with CANX and B2M through co-immunoprecipitation. The results showed that knocking down *B4GALT5* significantly enhanced the binding of HLA-A with CANX and B2M (figure 4H; online supplemental figure S4D), indicating a substantial increase in mature HLA-A levels. Conversely, overexpression of B4GALT5 significantly reduced the binding of HLA-A with CANX and B2M (figure 4I; online supplemental figure S4E).

Given that B4GALT5 has galactosyltransferase activity and that the proper folding of MHC-I is dependent on its glycosylation,[35] we explored whether B4GALT5 influences the glycosylation of HLA-A, thereby leading to its degradation. In AsPC-1 cells, after knocking down *B4GALT5*, we assessed HLA-A glycosylation using a biotinylated WGA lectin via Co-IP. The results showed that knocking down *B4GALT5* did not affect the glycosylation of HLA-A (online supplemental figure S4F). Furthermore, we constructed a mutant plasmid where the 110th N residue of HLA-A was mutated to Q to prevent normal glycosylation. We transfected MIA-PaCa-2 cells with control plasmid, HLA-A-Flag, and HLA-A(N110Q)-Flag expression plasmids and found through Co-IP that the glycosylation site mutation prevented HLA-A from binding to CANX and B2M, but did not affect its binding with B4GALT5 (online supplemental figure S4G). Therefore, these results indicate that the interaction between B4GALT5 and HLA-A occurs before the glycosylation of HLA-A. Since the degradation of HLA-A in the ER mainly occurs via the ERAD pathway, we next used Co-IP to examine the entry of HLA-A into the ERAD pathway following the knocking down or increasing *B4GALT5*. Knocking down *B4GALT5* significantly reduced the binding of HLA-A to key ERAD pathway molecules VCP and HRD1 (figure 4J; online supplemental figure S3H), whereas overexpression of *B4GALT5* significantly increased their binding (figure 4K; online supplemental figure S4I). This indicates that the entry of HLA-A2 into the ERAD pathway for degradation was reduced.

These results collectively revealed that the interaction between B4GALT5 and immature HLA-A in the ER affects

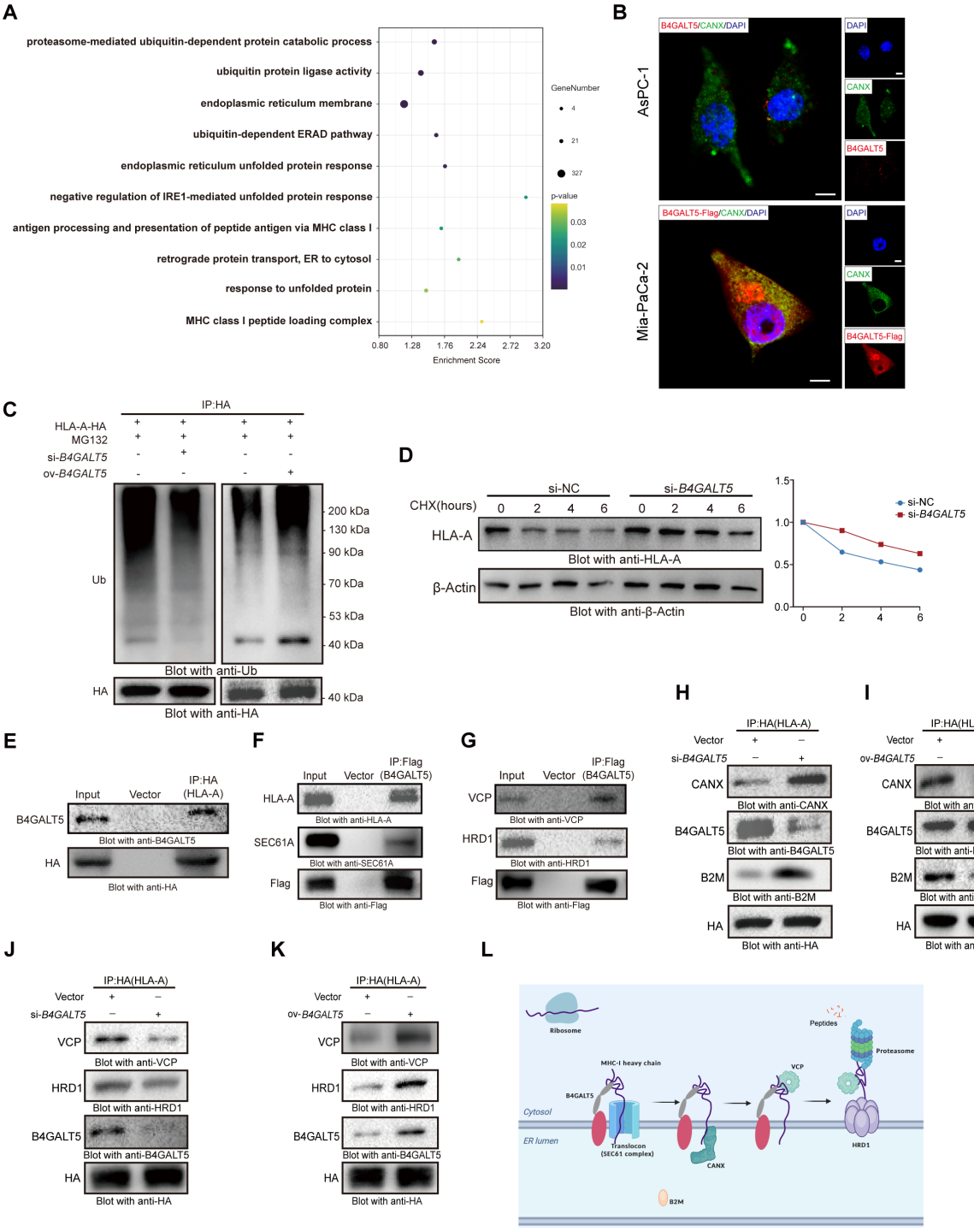

Figure 4 B4GALT5 regulates MHC-I via ERAD. (A) GO-BP enrichment analysis based on RNA sequencing data of AsPC-1 cells in si-NC and si-*B4GALT5* groups. (B) Colocalization of B4GALT5 with CANX in AsPC-1 (up: endogenous B4GALT5 expression) and MIA-PaCa-2 (down: exogenous B4GALT5) cells. (C) After knocking down or overexpressing *B4GALT5* in AsPC-1 cells stably expressing HLA-A-HA, cells were treated with MG132 (10 µM) for 8 hours, immunoprecipitated with the HA antibody and immunoblotted with the ubiquitin antibody. (D) In AsPC-1 cells, after knocking down *B4GALT5* expression, cells were treated with cycloheximide (10 µM) for 0, 2, 4, or 6 hours, and the half-life of HLA-A was detected by western blotting. Right: quantitative estimates of class I HLA levels based on western blot analyses. (E–G) Co-IP detection of the interactions between B4GALT5 and HLA-A, SEC61A, VCP, and HRD1. (H–I) After knocking down B4GALT5 expression in AsPC-1 cells (H), and overexpressing B4GALT5 in MIA-PaCa-2 cells (I), the binding of HLA-A with CANX and B2M was detected by Co-IP. (J–K) After knocking down *B4GALT5* expression in AsPC-1 cells (J), and overexpressing *B4GALT5* in MIA-PaCa-2 cells (K), the binding of HLA-A with VCP and HRD1 was detected by Co-IP. (L) A model depicting the functional mechanism of B4GALT5 downregulating HLA-A via the ERAD pathway in pancreatic ductal adenocarcinoma. B4GALT5, beta-1,4-galactosyltransferase-5; GO-BP, gene ontology-biological process; CANX, calnexin; Co-IP, co-immunoprecipitation; ER, endoplasmic reticulum; ERAD, endoplasmic reticulum-associated degradation; MHC, major histocompatibility complex.

HLA-A's association with CANX and B2M, promoting its degradation through the ERAD pathway (figure 4L).

B4GALT5 inhibits the cytotoxicity of CD8+ T cells by suppressing MHC-I *in vitro*

To determine the impact of B4GALT5 on CD8+ T cell cytotoxicity in PDAC cells, we constructed OVA-overexpressing murine PDAC cell lines KPC1199 and PANC02 using lentiviral vector-OVA. The $OVA_{257-264}$ (SIINFEKL) antigen peptide can be presented on the cell surface by H-2Kb and is specifically recognized by CD8+ T cells from OT-I mice.[36] We then knocked down *B4galt5* expression in these KPC1199 and PANC02 cells. Flow cytometry analysis showed that knockdown of *B4galt5* significantly increased the levels of SIINFEKL-H-2Kb on the surface of murine PDAC cells compared with the NC group (online supplemental figure S5A,B).

To further verify whether the regulation of MHC-I by B4GALT5 affects the function of CD8+ T cells, we conducted a co-culture experiment with OVA-Tumor cells and OT-1 CD8+ T cells. We first measured the levels of GZMB, IFN-γ, and TNF-α in the supernatants of OT-1 CD8+ T cells co-cultured with tumor cells expressing different levels of B4GALT5 by ELISA assay. The results showed that, compared with the NC group, the *B4galt5* knockdown group exhibited significantly higher levels of GZMB, IFN-γ, and TNF-α in the supernatant, indicating that *B4galt5* knockdown enhances the cytotoxicity of CD8+ T cells (figure 5A,B). Next, we analyzed the tumor cell apoptosis after co-culture with OT-1 CD8+ T cells using flow cytometry. The results showed that the *B4galt5* group knockdown group exhibited a significant increase in apoptotic tumor cells compared with the sh-NC group (figure 5C,D). Meanwhile, we assessed tumor cell viability using the CCK8 assay. The results indicated that tumor cells in the *B4galt5* knockdown group exhibited a significantly reduced survival rate compared with the sh-NC group (figure 5E,F). Microscopic observations further supported this finding, showing that *B4galt5* knockdown significantly enhances the cytotoxic effect of CD8+ T cells against tumor cells (online supplemental figure S5D,E). Additionally, blocking SIINFEKL ($OVA_{257–264}$ antigen peptide) significantly reversed this enhanced CD8+ T cell-mediated cytotoxic effect, further confirming that this phenomenon is MHC-I dependent (figure 5G,H). In summary, these results indicate that *B4galt5* knockdown enhances CD8+ T cell-mediated tumor cytotoxicity by upregulating MHC-I levels *in vitro*.

B4GALT5 inhibits the expression of MHC-I and CD8+ T-cell infiltration in mouse tumor models and clinical samples

We assessed immune cell scores in PDAC samples from the TCGA-PDAC cohort using CIBERSORT and performed correlation analysis. The results demonstrated that B4GALT5 expression was significantly negatively correlated with CD8+ T-cell infiltration in PDAC patients (online supplemental figure S6A). Furthermore, we analyzed the correlation between B4GALT5 expression and MHC-I levels in tumor tissues of PDAC patients using IHC. The results showed that, compared with patients with high B4GALT5 expression, patients with low B4GALT5 expression exhibited significantly higher levels of MHC-I in tumor tissues (figure 6A). Additionally, we used mIHC to examine the infiltration of CD8+ GZMB+ T cells in tumor tissues of patients with PDAC with different B4GALT5 expression levels. The results indicated that patients with low B4GALT5 expression had significantly higher levels of CD8+ GZMB+ T-cell infiltration in tumor tissues (figure 6B). To further validate these findings, we examined the correlation between B4GALT5 and tumor-infiltrating CD8+ T cells in a murine PDAC orthotopic model using flow cytometry and immunofluorescence. The results showed that knockdown of *B4galt5* significantly increased CD8+ T-cell infiltration in tumor tissues (figure 6C and online supplemental figure S6B–E). Furthermore, we assessed the cytokine secretion capacity of CD8+ T cells and found that tumor-infiltrating CD8+ T cells in the *B4galt5* knockdown group exhibited significantly higher expression levels of GZMB, TNF-α, and IFN-γ (figure 6D and online supplemental figure S6F), further supporting the role of B4GALT5 in regulating immune responses within the tumor microenvironment.

Furthermore, to check the role of B4GALT5 in influencing the CD8+ T cells is MHC-I dependent, we blocked MHC-I-mediated antigen presentation using an H-2Kb antibody in the murine PDAC model and evaluated the impact of *B4galt5* knockdown on tumor progression *in vivo*. The results demonstrated that blocking MHC-I reversed the tumor growth inhibition effect induced by *B4galt5* knockdown (figure 6E,F), indicating that B4GALT5 influences tumor immune evasion by regulating MHC-I-mediated antigen presentation, thereby modulating CD8+ T cell-mediated antitumor immune responses.

Finally, based on recently published single-cell sequencing data from PDAC,[37 38] we performed single-cell clustering analysis to compare B4GALT5 expression in tumor cells of untreated and neoadjuvant-treated patients with PDAC. The results revealed that B4GALT5 expression was significantly reduced in tumor cells following neoadjuvant treatment (figure 6G,H), suggesting that B4GALT5 may play a crucial role in PDAC immune evasion and that its expression could be influenced by therapy.

DISCUSSION

Immune surveillance is considered a crucial protective mechanism for the host to suppress the occurrence and development of tumors and maintain intracellular homeostasis. Initially, newly transformed tumor cells can be eliminated through innate immune responses, such as natural killer cells. However, during the progression of the tumor, even though antigen-specific T cells can trigger an adaptive immune response, the selection by the immune system can induce mutations in tumor cells, such as the

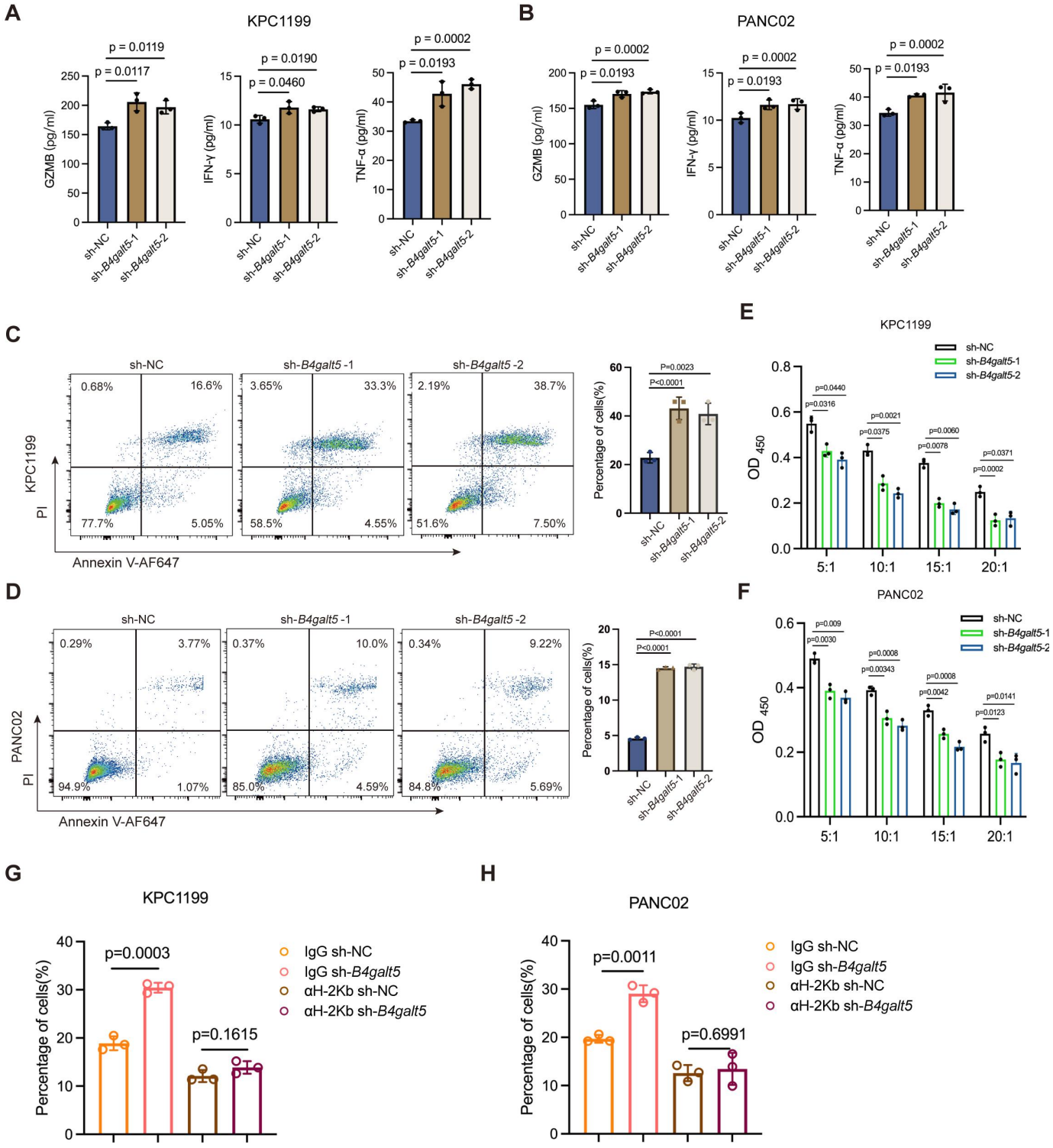

Figure 5 Beta-1,4-galactosyltransferase-5 inhibits the cytotoxicity of CD8$^+$ T cells *in vitro* by suppressing major histocompatibility complex-I. (A–B) ELISA was used to detect the levels of GZMB, IFN-γ, and TNF-α in the supernatant of co-cultures of KPC1199-OVA (A) and PANC02-OVA (B) cells with OT-1 CD8$^+$ T cells for 12 hours. n=3 per group. (C–D) OT-1 mouse CD8$^+$ T cells were co-cultured with OVA-KPC1199 (C) or OVA-PANC02 (D) for 12 hours, and then flow cytometry was used to assess the levels of apoptosis of the tumor cells (CD8$^+$ T cells: tumor cells=5:1; n=3 per group). Three independent experiments. (E–F) Different ratios of CD8$^+$ T cells were co-cultured with KPC1199-OVA (E) or PANC02-OVA (F) (ratios: 5:1, 10:1, 15:1, 20:1) for 24 hours, and then CCK8 assay was used to assess tumor cell viabilities. n=3 per group, three independent experiments. (G–H) OT-1 mouse CD8$^+$ T cells were co-cultured with KPC1199-OVA (G) or PANC02-OVA (H) and treated with αSIINFEKL antibody for 12 hours, followed by flow cytometry analysis to assess tumor cell apoptosis (CD8$^+$ T cells: tumor cells=5:1; n=3 per group). Three independent experiments. Bars represent mean±SD. The p values shown were calculated using an unpaired t-test. GZMB, granzyme B; IFN, interferon; TNF, tumor necrosis factor.

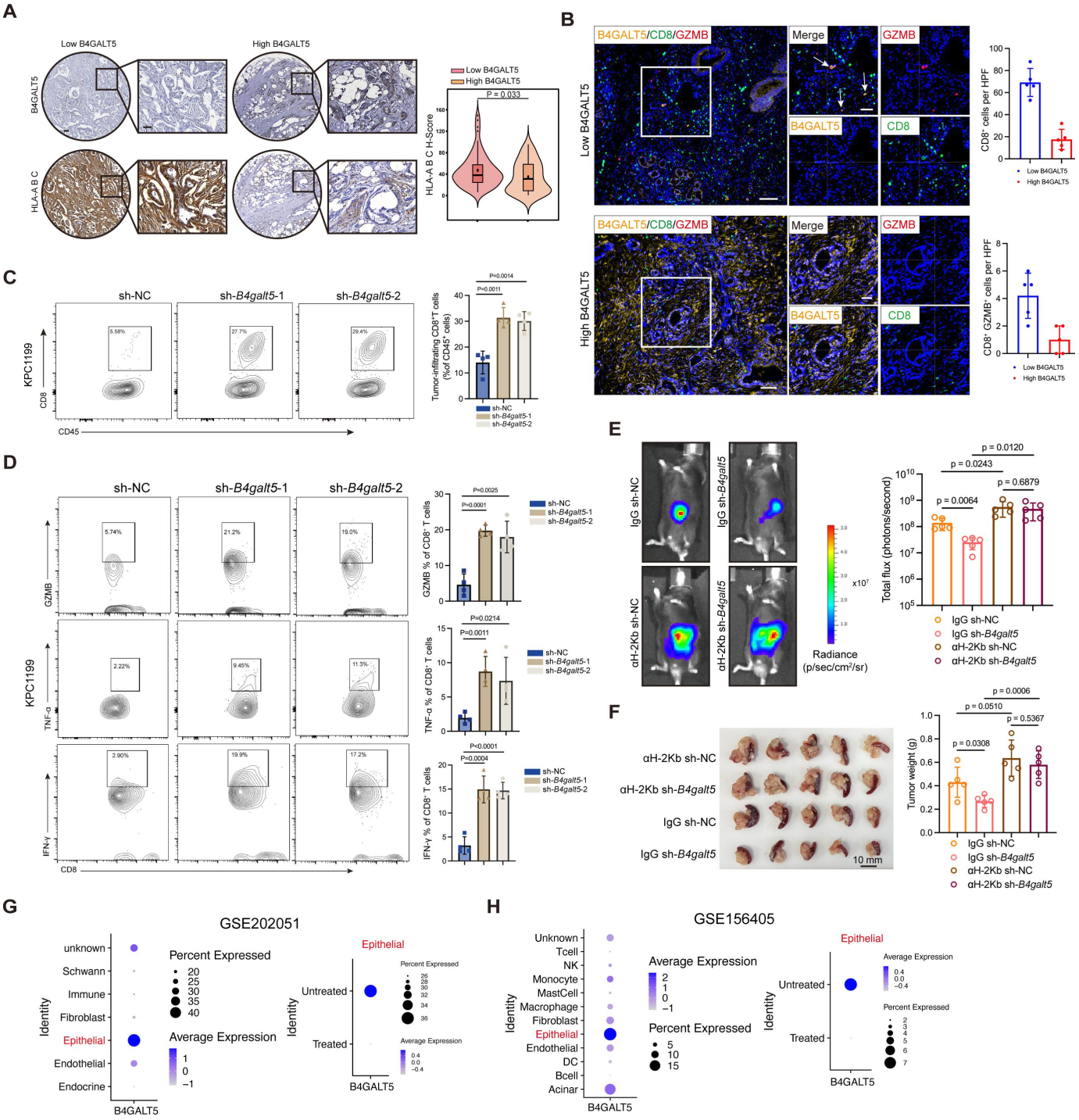

Figure 6 B4GALT5 inhibits CD8⁺ T-cell infiltration in mouse models. (A) Left: representative immunohistochemistry staining results demonstrated significant differences in MHC-I staining in tumor tissues from tissue microarrays of patients with PDAC with high and low B4GALT5 expression. Scale bars: 100 µm (left); 50 µm (right). Right: HLA-A B C expression between patients with low and high expression levels of B4GALT5 was compared. Two-tailed t-test. (B) Multiplexed immunohistochemistry was used to detect the levels of CD8⁺ GZMB⁺ T cells (shown in white arrow) in tumor tissues of patients with PDAC with low B4GALT5 (up) and high B4GALT5 (down) expression. Scale bars: 100 µm (left); 50 µm (right). (C) Flow cytometry analysis of GZMB, TNF-α, and IFN-γ levels within tumor-infiltrating CD8⁺ T cells in tumor tissues from different groups (sh-NC, sh-*B4galt5*) with orthotopic PDAC models of KPC1199 mice (n=4 per group). (E–F) The Living Image system was used to observe tumor progression in an orthotopic PDAC mouse model constructed with KPC1199 cells after αH-2Kb blockade (E). Tumor size and weight were measured after αH-2Kb treatment (F). n=5, per group. (G–H) *B4GALT5* expression across different cell types and treatment conditions of pancreatic cancer patients in the Gene Expression Omnibus data sets GSE202051 (G) and GSE156405 (H). Left: *B4GALT5* expression across various cell types. Right: *B4GALT5* expression of epithelial cells between the treatment and non-treatment groups. B4GALT5, beta-1,4-galactosyltransferase-5; IFN, interferon; MHC, major histocompatibility complex; PDAC, pancreatic ductal adenocarcinoma.

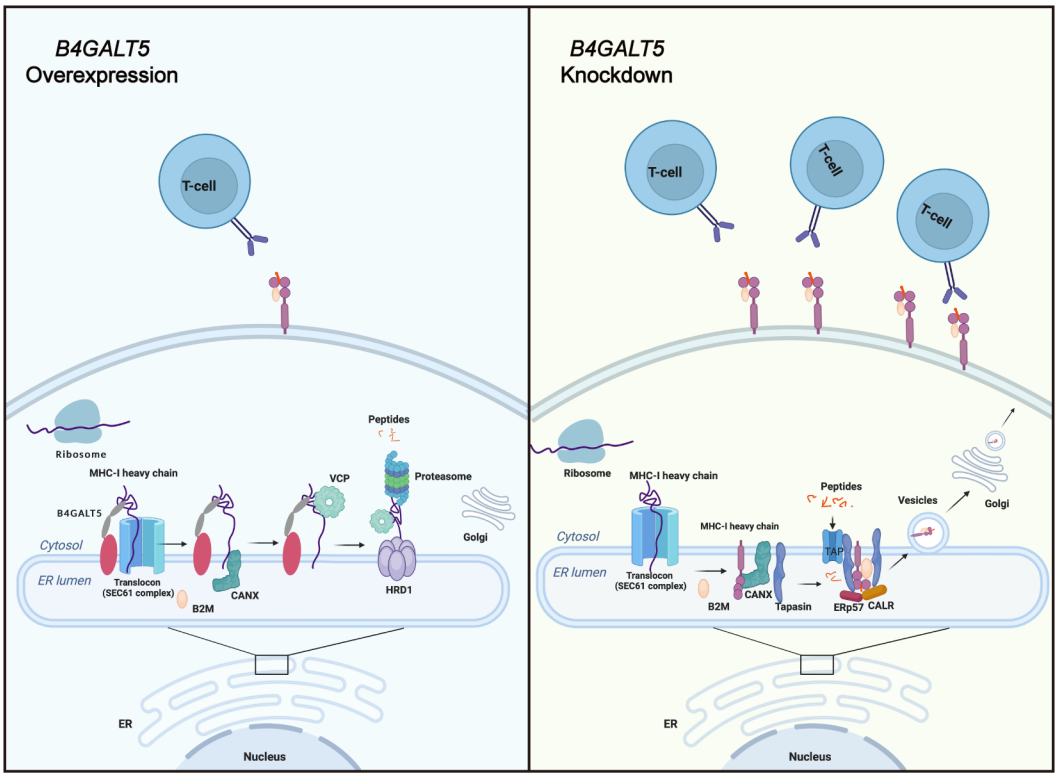

Figure 7 Inhibition of B4GALT5 restores surface MHC-I expression by preventing B4GALT5-mediated MHC-I degradation through the endoplasmic reticulum-associated degradation pathway, thereby promoting CD8$^+$ T-cell infiltration and enhancing its antitumor effect against pancreatic ductal adenocarcinoma. B2M, beta-2 microglobulin; B4GALT5, beta-1,4-galactosyltransferase-5; CANX, calnexin; ER, endoplasmic reticulum; MHC, major histocompatibility complex.

loss of MHC-I molecules, preventing tumor antigens from being presented on the cell surface, making tumor cells unrecognizable by the immune system, thereby allowing immune cells to evade the body's immune attack.[39–41] In this study, based on the "antigen processing and presentation of peptide antigen via MHC-I" gene signature, we identified four DEGs negatively associated with it. Among these, we verified that B4GALT5 was a crucial factor in PDAC cells for inhibiting MHC-I expression, leading to impaired antitumor CD8$^+$ T-cell responses in the tumor microenvironment. Our study demonstrates that B4GALT5 interacts with MHC-I, thereby enhancing the binding of MHC-I to the key ERAD pathway molecules VCP and HRD1, promoting its ubiquitination and accelerating its degradation, ultimately leading to a reduction in overall MHC-I levels. This process decreases MHC-I expression on the tumor cell membrane, thereby impairing the activation of CD8$^+$ T cells in the tumor microenvironment and weakening their antitumor immune response (figure 7).

Under normal physiological conditions, the HC of the MHC-I molecule, once translated on ribosomes, enters the ER with the help of the SEC61 complex, where the HC is in an unfolded state. In the ER, the HC binds with molecular chaperones and glycosylation-related enzymes to form a properly folded glycoprotein. The formation of HC-B2M dimers signifies the maturation of MHC-I molecules. Only mature MHC-I molecules can assemble with peptides transported by tapasin to be presented on the cell surface for recognition by CD8$^+$ T cells.[35 42 43] Our study indicates that B4GALT5 interacts with HLA-A and the expression of B4GALT5 is negatively correlated with HLA-A, knocking down B4GALT5 can significantly restore the expression level of MHC-I molecules in PDAC cells. Given the glycosyltransferase activity inherent in B4GALT5, we previously suspected that this phenomenon was caused by the enzymatic activity of B4GALT5. Therefore, we knocked down B4GALT5 in PDAC cells and then tested the glycosylation level of HLA-A. Surprisingly, this change did not alter the glycosylation level of HLA-A. Furthermore, we also mutated the glycosylation sites of HLA-A, consistent with previous study reports, mutated HLA-A could not bind with the molecular chaperone CANX or B2M. But we found that the mutated glycosylation site HLA-A still interacts with B4GALT5. These findings thus suggest that the effect of B4GALT5 on MHC-I is not due to its enzymatic activity.

To investigate how B4GALT5 inhibits the expression of MHC-I in PDAC cells, we conducted mass spectrometry and immunoprecipitation analyses and found that B4GALT5 interacts with VCP, a key molecule in the ERAD pathway. Previous studies have reported that MHC-I will enter the ERAD pathway to maintain the homeostasis of the ER, if MHC-I on the ER cannot fold correctly or undergo proper glycosylation modifications.[6] As a core element of the ubiquitin-proteasome system, VCP plays a crucial role in ERAD. During dislocation from the ER, misfolded or misassembled MHC-I HC are recognized by VCP and pulled out,

transported to the cytoplasm, ubiquitinated on the cytoplasmic side of the ER membrane, and degraded by the cytoplasmic proteasome.[44 45] Our study demonstrates that in the presence of B4GALT5, more HLA-A is directed towards the ERAD pathway for degradation. Meanwhile, knocking down *B4GALT5* significantly enhances the binding of HLA-A with CANX and B2M, thereby promoting the maturation of MHC-I expression.

According to previous reports, the antigen presentation of MHC-I determines the specificity of $CD8^+$ T cells.[7 46 47] Thus, we co-cultured OT-1 $CD8^+$ T cells with OVA-Tumor cells *in vitro* to mimic the biological process of antigen presentation mediated by MHC-I in tumor cells recognized by $CD8^+$ T cells. Under conditions of B4GALT5 knockdown, the cytotoxic effects of $CD8^+$ T cells against tumor cells were significantly enhanced. We also constructed an in situ mouse PDAC model to validate the impact of B4GALT5 on the quantity and activity of tumor-infiltrating $CD8^+$ T cells *in vivo*. The results also showed that knocking down *B4galt5* significantly increased the number of tumor-infiltrating $CD8^+$ T cells, and they produced more GZMB, IFN-γ and TNF-α, indicating increased cytotoxicity against tumor cells.

In summary, MHC-I holds broad prospects in tumor immunotherapy, especially in intractable cancers like PDAC. By enhancing HLA-A expression and function, significant enhancements in immunotherapy effectiveness can be achieved, overcoming the current limitations of immune checkpoint blockade (ICB) therapy and providing better treatment outcomes for patients.[48–50] Our study has identified B4GALT5 as a crucial factor inhibiting MHC-I expression in PDAC cells, providing a promising target for further immunotherapy in PDAC.

Author affiliations
[1]Shanghai Fengxian District Central Hospital, School of Medicine, Anhui University of Science and Technology, Shanghai, China
[2]Shanghai University of Medicine and Health Sciences Affiliated Sixth People's Hospital South Campus, Shanghai, China
[3]State Key Laboratory of Systems Medicine for Cancer, Shanghai Cancer Institute, Ren Ji Hospital, School of Medicine, Shanghai Jiao Tong University, Shanghai, China
[4]The First Hospital of Jilin University, Changchun, Jilin, China
[5]Department of Gastrointestinal Surgery, Renji Hospital, School of Medicine, Shanghai Jiao Tong University, Shanghai, China
[6]Department of Biliary-Pancreatic Surgery, Ren Ji Hospital, School of Medicine, Shanghai Jiao Tong University, Shanghai, China

Acknowledgements Special thanks to Professor Jing Xue for generously providing mouse KPC1199 and PANC02 cells and to Professor Yongzhong Liu for providing OT-1 mice.

Contributors Conception and design: XX, S-QY, X-QL, X-MY, X-LZ. Development of methodology: S-QY, H-TM, S-YX, AT, X-QL. Analysis and interpretation of data: S-QY, XX, HL, X-QL Y-TL, HZ. Writing, review, and/or revision of the manuscript: S-QY, XX, YY, Y-MH, HL, ZZ, X-LZ. Administrative, technical, or material support: XX, X-MY, YY, X-LZ. Guarantor: X-LZ

Funding The study was supported by the Scientific Research Foundation of SUMHS (No. SSF-23-15-002 to XX), Natural Science Foundation of Shanghai (No. 22ZR1460000 to X-LZ). Innovative research team of high-level local universities in Shanghai (SHSMU-ZDCX20210802), Key Medical Disciplines of Shanghai Municipal Health Commission (2024ZDXK0045 and 2024ZDXK0015).

Competing interests None declared.

Patient consent for publication Not applicable.

Ethics approval The study was approved by the Research Ethics Committee of Ren Ji Hospital, School of Medicine, Shanghai Jiao Tong University (ID: 2015037). Participants gave informed consent to participate in the study before taking part.

Provenance and peer review Not commissioned; externally peer reviewed.

Data availability statement Data are available upon reasonable request.

ORCID iDs
Xin Xing http://orcid.org/0000-0002-4766-4926
Xue-Li Zhang http://orcid.org/0000-0001-8306-0639

REFERENCES

1 Mizrahi JD, Surana R, Valle JW, *et al*. Pancreatic cancer. *Lancet* 2020;395:2008–20.
2 Wood LD, Canto MI, Jaffee EM, *et al*. Pancreatic Cancer: Pathogenesis, Screening, Diagnosis, and Treatment. *Gastroenterology* 2022;163:386–402.
3 Yamamoto K, Venida A, Yano J, *et al*. Autophagy promotes immune evasion of pancreatic cancer by degrading MHC-I. *Nature New Biol* 2020;581:100–5.
4 Sang W, Zhou Y, Chen H, *et al*. Receptor-interacting Protein Kinase 2 Is an Immunotherapy Target in Pancreatic Cancer. *Cancer Discov* 2024;14:326–47.
5 Dersh D, Hollý J, Yewdell JW. A few good peptides: MHC class I-based cancer immunosurveillance and immunoevasion. *Nat Rev Immunol* 2021;21:116–28.
6 Wang Y, Wang X, Cui X, *et al*. Oncoprotein SND1 hijacks nascent MHC-I heavy chain to ER-associated degradation, leading to impaired CD8+ T cell response in tumor . *Sci Adv* 2020;6:eaba5412.
7 Chen X, Lu Q, Zhou H, *et al*. A membrane-associated MHC-I inhibitory axis for cancer immune evasion. *Cell* 2023;186:3903–20.
8 Silva MC, Fernandes Â, Oliveira M, *et al*. Glycans as Immune Checkpoints: Removal of Branched N-glycans Enhances Immune Recognition Preventing Cancer Progression. *Cancer Immunol Res* 2020;8:1407–25.
9 Wolfert MA, Boons G-J. Adaptive immune activation: glycosylation does matter. *Nat Chem Biol* 2013;9:776–84.
10 Li Y, Lin Y, Aye L, *et al*. An integrative pan-cancer analysis of the molecular and biological features of glycosyltransferases. *Clin Transl Med* 2022;12:e872.
11 Mugisha S, Di X, Disoma C, *et al*. Fringe family genes and their modulation of Notch signaling in cancer. *Biochimica et Biophysica Acta (BBA) - Reviews on Cancer* 2022;1877:188746.
12 Li C-W, Lim S-O, Chung EM, *et al*. Eradication of Triple-Negative Breast Cancer Cells by Targeting Glycosylated PD-L1. *Cancer Cell* 2018;33:187–201.
13 Pinho SS, Reis CA. Glycosylation in cancer: mechanisms and clinical implications. *Nat Rev Cancer* 2015;15:540–55.
14 Amado M, Almeida R, Schwientek T, *et al*. Identification and characterization of large galactosyltransferase gene families: galactosyltransferases for all functions. *Biochimica et Biophysica Acta (BBA) - General Subjects* 1999;1473:35–53.
15 Li S-F, Zhu C-S, Wang Y-M, *et al*. Downregulation of β1,4-galactosyltransferase 5 improves insulin resistance by promoting adipocyte commitment and reducing inflammation. *Cell Death Dis* 2018;9:196.
16 Cui S, Zhang X, Li Y, *et al*. UGCG modulates heart hypertrophy through B4GalT5-mediated mitochondrial oxidative stress and the ERK signaling pathway. *Cell Mol Biol Lett* 2023;28:71.

17 Wang Q, Zhou S, Hu X, *et al*. Circadian Genes MBOAT2/CDA/LPCAT2/B4GALT5 in the Metabolic Pathway Serve as New Biomarkers of PACA Prognosis and Immune Infiltration. *Life (Basel)* 2023;13:1116.
18 Zhao R, Zhou Y, Shi H, *et al*. Effect of Gestational Diabetes on Postpartum Depression-like Behavior in Rats and Its Mechanism. *Nutrients* 2022;14:1229.
19 Yin J-Z, Shi X-Q, Wang M-D, *et al*. Arsenic trioxide elicits anti-tumor activity by inhibiting polarization of M2-like tumor-associated macrophages via Notch signaling pathway in lung adenocarcinoma. *Int Immunopharmacol* 2023;117:109899.
20 Hänzelmann S, Castelo R, Guinney J. GSVA: gene set variation analysis for microarray and RNA-seq data. *BMC Bioinformatics* 2013;14:7.
21 Böhm CM, Hanski ML, Stefanović S, *et al*. Identification of HLA-A2-restricted epitopes of the tumor-associated antigen MUC2 recognized by human cytotoxic T cells. *Int J Cancer* 1998;75:688–93.
22 Riener M, Wild PJ, Soll C, *et al*. Frequent expression of the novel cancer testis antigen MAGE-C2/CT-10 in hepatocellular carcinoma. *Intl Journal of Cancer* 2009;124:352–7.
23 Oria VO, Lopatta P, Schilling O. The pleiotropic roles of ADAM9 in the biology of solid tumors. *Cell Mol Life Sci* 2018;75:2291–301.
24 Nawrocki ST, Olea J, Villa Celi C, *et al*. Comprehensive Single-Cell Immune Profiling Defines the Patient Multiple Myeloma Microenvironment Following Oncolytic Virus Therapy in a Phase Ib Trial. *Clin Cancer Res* 2023;29:5087–103.
25 Yang M-W, Tao L-Y, Jiang Y-S, *et al*. Perineural Invasion Reprograms the Immune Microenvironment through Cholinergic Signaling in Pancreatic Ductal Adenocarcinoma. *Cancer Res* 2020;80:1991–2003.
26 Ellsworth KA, Eckloff BW, Li L, *et al*. Contribution of FKBP5 genetic variation to gemcitabine treatment and survival in pancreatic adenocarcinoma. *PLoS One* 2013;8:e70216.
27 Zhang G, He P, Tan H, *et al*. Integration of metabolomics and transcriptomics revealed a fatty acid network exerting growth inhibitory effects in human pancreatic cancer. *Clin Cancer Res* 2013;19:4983–93.
28 Tong Y, Sun M, Chen L, *et al*. Proteogenomic insights into the biology and treatment of pancreatic ductal adenocarcinoma. *J Hematol Oncol* 2022;15:168.
29 Frontiers Editorial Office. Retraction: ECT2 Increases the Stability of EGFR and Tumorigenicity by Inhibiting Grb2 Ubiquitination in Pancreatic Cancer. *Front Oncol* 2021;11:734761.
30 Albahde MAH, Zhang P, Zhang Q, *et al*. Upregulated Expression of TUBA1C Predicts Poor Prognosis and Promotes Oncogenesis in Pancreatic Ductal Adenocarcinoma via Regulating the Cell Cycle. *Front Oncol* 2020;10:49.
31 Foster DS, Januszyk M, Delitto D, *et al*. Multiomic analysis reveals conservation of cancer-associated fibroblast phenotypes across species and tissue of origin. *Cancer Cell* 2022;40:1392–406.
32 Wiertz EJ, Tortorella D, Bogyo M, *et al*. Sec61-mediated transfer of a membrane protein from the endoplasmic reticulum to the proteasome for destruction. *Nature New Biol* 1996;384:432–8.
33 Araki K, Nagata K. Protein folding and quality control in the ER. *Cold Spring Harb Perspect Biol* 2011;3:a007526.
34 Claessen JHL, Kundrat L, Ploegh HL. Protein quality control in the ER: balancing the ubiquitin checkbook. *Trends Cell Biol* 2012;22:22–32.
35 Chong C, Coukos G, Bassani-Sternberg M. Identification of tumor antigens with immunopeptidomics. *Nat Biotechnol* 2022;40:175–88.
36 Lutz V, Hellmund VM, Picard FSR, *et al*. IL18 Receptor Signaling Regulates Tumor-Reactive CD8+ T-cell Exhaustion via Activation of the IL2/STAT5/mTOR Pathway in a Pancreatic Cancer Model. *Cancer Immunol Res* 2023;11:421–34.
37 Boucher Y, Posada JM, Subudhi S, *et al*. Addition of Losartan to FOLFIRINOX and Chemoradiation Reduces Immunosuppression-Associated Genes, Tregs, and FOXP3+ Cancer Cells in Locally Advanced Pancreatic Cancer. *Clin Cancer Res* 2023;29:1605–19.
38 Lee JJ, Bernard V, Semaan A, *et al*. Elucidation of Tumor-Stromal Heterogeneity and the Ligand-Receptor Interactome by Single-Cell Transcriptomics in Real-world Pancreatic Cancer Biopsies. *Clin Cancer Res* 2021;27:5912–21.
39 Wu X, Li T, Jiang R, *et al*. Targeting MHC-I molecules for cancer: function, mechanism, and therapeutic prospects. *Mol Cancer* 2023;22:194.
40 Luo X, Qiu Y, Fitzsimonds ZR, *et al*. Immune escape of head and neck cancer mediated by the impaired MHC-I antigen presentation pathway. *Oncogene* 2024;43:388–94.
41 Garrido F, Aptsiauri N. Cancer immune escape: MHC expression in primary tumours versus metastases. *Immunology* 2019;158:255–66.
42 Perosa F, Luccarelli G, Prete M, *et al*. Beta 2-microglobulin-free HLA class I heavy chain epitope mimicry by monoclonal antibody HC-10-specific peptide. *J Immunol* 2003;171:1918–26.
43 Kukita K, Tamura Y, Tanaka T, *et al*. Cancer-Associated Oxidase ERO1-α Regulates the Expression of MHC Class I Molecule via Oxidative Folding. *J Immunol* 2015;194:4988–96.
44 Römisch K. A Case for Sec61 Channel Involvement in ERAD. *Trends Biochem Sci* 2017;42:171–9.
45 Zimmermann C, Kowalewski D, Bauersfeld L, *et al*. HLA-B locus products resist degradation by the human cytomegalovirus immunoevasin US11. *PLoS Pathog* 2019;15:e1008040.
46 Taylor BC, Sun X, Gonzalez-Ericsson PI, *et al*. NKG2A Is a Therapeutic Vulnerability in Immunotherapy Resistant MHC-I Heterogeneous Triple-Negative Breast Cancer. *Cancer Discov* 2024;14:290–307.
47 Beck JD, Diken M, Suchan M, *et al*. Long-lasting mRNA-encoded interleukin-2 restores $CD8^+$ T cell neoantigen immunity in MHC class I-deficient cancers. *Cancer Cell* 2024;42:568–82.
48 Benci JL, Johnson LR, Choa R, *et al*. Opposing Functions of Interferon Coordinate Adaptive and Innate Immune Responses to Cancer Immune Checkpoint Blockade. *Cell* 2019;178:933–48.
49 Liu D, Schilling B, Liu D, *et al*. Integrative molecular and clinical modeling of clinical outcomes to PD1 blockade in patients with metastatic melanoma. *Nat Med* 2019;25:1916–27.
50 Cheung PF, Yang J, Fang R, *et al*. Progranulin mediates immune evasion of pancreatic ductal adenocarcinoma through regulation of MHCI expression. *Nat Commun* 2022;13.